Extreme Mechanics Letters 25 (2018) 37–44

Contents lists available at ScienceDirect

Extreme Mechanics Letters

journal homepage: www.elsevier.com/locate/eml

A viscoelastic beam theory of polymer jets with application to rotary jet spinning

Qihan Liu, Kevin Kit Parker *

Disease Biophysics Group, Wyss Institute for Biologically Inspired Engineering, John A. Paulson School of Engineering and Applied Science, Harvard University, Cambridge, MA 02138, United States

ARTICLE INFO

Article history:
Received 8 August 2018
Received in revised form 15 October 2018
Accepted 15 October 2018
Available online 30 October 2018

Keywords:
Viscoelasticity
Beam
Oldroyd-B
Polymer jet
Centrifugal force
Rotary jet spinning

ABSTRACT

Complex deformation of a polymer jet appears in many manufacturing processes, such as 3D printing, electrospinning, blow spinning, and rotary jet spinning. In these applications, a polymer melt or solution is first extruded through an orifice and forms a jet. The polymer jet is then dynamically deformed until the polymer solidifies. The final product is strongly affected by the deformation of the polymer jet. And the deformation is strongly affected by the viscoelasticity of the polymer. Here we develop a beam theory to incorporate both the nonlinear viscoelasticity and the bending/twisting stiffness of a polymer jet. As a demonstration, we study the formation of a polymer fiber under strong centrifugal force, a fiber manufacturing process known as rotary jet spinning.

Published by Elsevier Ltd.

1. Introduction

Extruding polymer melt and solution through an orifice forms a polymer jet. Polymer jets are involved in many manufacturing processes, such as plastic extrusion [1], conventional dry/wet/melt spinning [2,3], 3D printing [4], electrospinning [5,6], blow spinning [7,8], and rotary jet spinning [9–14]. In many applications, the polymer jet undergoes complex deformation before it solidifies. For example, in 3D printing, the coiling of the polymer jet is harnessed to print complex patterns [15]. In electrospinning, the charged jet undergoes chaotic whipping motion which elongates the jet into a nanofiber [16]. In blow spinning, the polymer jet flaps in the high speed airflow during elongation [17,18]. In rotary jet spinning, the polymer jet is elongated by centrifugal force where bending is induced by Coriolis force and air-drag [9,19]. In these applications, the deformation history of the polymer jet determines the geometry and the microstructure of the final product. Understanding how the processing parameters affect the deformation of the polymer jet is crucial to the development of the manufacturing processes. The search for such understanding motivates the modeling of polymer jets.

In the existing literature, a polymer jet is often modeled as a thin string with no bending stiffness or twisting stiffness. The string model is popular for its mathematical simplicity [17,19–27]. However, neglecting bending and twisting fail the modeling in certain applications. For example, in 3D printing, a polymer jet must be under compression to coil. A string model is impossible to predict coiling under compression [28,29]. Such coiling is also observed in electrospinning near the collector [30]. As another example, during rotatory jet spinning, the polymer jet may be acutely bended near the orifice. The string model is known to diverge in this case [31–34]. For these applications, a polymer jet must be modeled as a beam with finite stiffness towards bending and twisting to correctly predict the deformation. However, since the beam models are mathematically more demanding than the string models, existing beam models are limited to simple material behaviors, such as linear viscosity [32,35,36], linear elasticity [37,38], nonlinear elasticity [39–41], or linear viscoelasticity [42–44]. A beam theory of more complex material behavior such as nonlinear viscoelasticity remains lacking. On the other hand, nonlinear viscoelasticity is often prominent for polymer jets, which are polymer solution or polymer melts undergoing large deformation. As a result, manufacturing processes like 3D printing and rotary jet spinning cannot be accurately modeled in lack of a beam model of nonlinearly viscoelastic material.

In this paper, we develop a beam theory that incorporates nonlinear viscoelasticity. Following the classical Euler–Bernoulli beam theory [45], we assume that a flat cross-section normal to the centerline to remain flat and normal, and approximate the deformation field to the first order of the thickness of the jet. In addition, we enforce the material incompressibility to the first order. The kinematics of finite deformation is derived following these assumptions. The kinematics is combined with a common nonlinear viscoelastic material model, the Oldroyd-B model [46,

* Correspondence to: 29 Oxford St. Pierce Hall 324, Cambridge, MA 02138, United States.
E-mail address: kkparker@seas.harvard.edu (K.K. Parker).

https://doi.org/10.1016/j.eml.2018.10.005
2352-4316/Published by Elsevier Ltd.

47], to derive the constitutive equations of a nonlinear viscoelastic beam. As a demonstration, the beam model is used to study the viscoelastic relaxation in rotary jet spinning [9,10].

The paper is organized as follows. Section 2 defines a local coordinate system that follows the movement of the jet. Section 3 derives the expression of the deformation field in the local coordinate system. Section 4 introduces the nonlinear viscoelastic model, Oldroyd-B model. The constitutive relation of a beam of Oldroyd-B material is derived. Section 5 derives the conservation laws of the beam model. Sections 3–5 completes the beam model. Section 6 introduces the rotary jet spinning platform. The model derived in previous sections is applied to study the viscoelastic relaxation in rotary jet spinning.

2. Local coordinate system of a polymer jet

A polymer jet is formed by extruding polymer solution, or polymer melt, through an orifice. We may choose an arbitrary spatial point in the orifice and mark all the material that passes through this point. The marked material forms a line that moves with the jet. We call this line the centerline of the jet, Fig. 1. Here we have not specified the exact spatial point in the orifice to define the centerline. The choice of centerline will be discussed later.

We define the lab frame of reference as a Cartesian coordinate system fixed in the lab space. We identify the spatial location of a material point on the centerline in the lab frame as $\mathbf{r}(s)$, Fig. 1A. Here s is the arc length of the centerline from the orifice. We have adopted the Eulerian description on the centerline, which means that s is always the current arc length and the same s generally corresponds to different materials points at different time. The unit tangent vector of the centerline is defined by

$$\mathbf{t} = \frac{\partial \mathbf{r}}{\partial s}. \tag{2.1}$$

Consider a material surface tangent to the centerline at the orifice, denote its unit normal vector as $\mathbf{n}$. As the jet extrudes and deforms, the material surface moves and deforms, but $\mathbf{n}$ remains perpendicular to the centerline and marks the orientation of the jet, Fig. 1A. We further define $\mathbf{b} = \mathbf{t} \times \mathbf{n}$. Vectors $\mathbf{t}, \mathbf{n}, \mathbf{b}$ form an orthogonal bases. The bases $\mathbf{t}, \mathbf{n}, \mathbf{b}$ rotate along the centerline. This rotation is characterized by the curvature vector $\boldsymbol{\kappa}$, with the definition

$$\boldsymbol{\kappa} \times \mathbf{l} = \frac{\partial \mathbf{l}}{\partial s}. \tag{2.2}$$

Here $\mathbf{l}$ is any one of $\mathbf{t}, \mathbf{n}, \mathbf{b}$. For each point on the centerline, $\mathbf{n}$ and $\mathbf{b}$ defines a cross-section of the jet, Fig. 1A. Any material point on the cross-section can be represented by an offset vector $\mathbf{h} = h_n\mathbf{n} + h_b\mathbf{b}$. The triplet (s, h_n, h_b) are the coordinates in the local frame of reference.

Viewing from the lab frame, the local frame moves with the jet. The velocity of a material point on the centerline is defined as

$$\mathbf{v} = \frac{D\mathbf{r}}{Dt}. \tag{2.3}$$

Here D/Dt means the time derivative following the same material point. The bases $\mathbf{t}, \mathbf{n}, \mathbf{b}$ fixed on a material point also rotate in time. This rotation is characterized by the angular velocity vector $\boldsymbol{\omega}$, defined by

$$\boldsymbol{\omega} \times \mathbf{l} = \frac{D\mathbf{l}}{Dt}. \tag{2.4}$$

Here $\mathbf{l}$ is any one of $\mathbf{t}, \mathbf{n}, \mathbf{b}$.

$\mathbf{t}$ and $\mathbf{v}$, or $\boldsymbol{\kappa}$ and $\boldsymbol{\omega}$ are kinematically related quantities. The differential equations describing the connections are derived in supplementary materials Section 1.

3. Deformation of a polymer jet

3.1. Reference state

The deformation of a material point is defined relative to a reference state. We identify the reference state of each material point as the state when the material point passes the orifice. The reference state reflects the loading history of a material point before the jet exits the orifice. Two material points in the jet may have different reference state, depending on the time and location that the material point passed through the orifice and the boundary condition at the orifice. Once the reference state is determined, we define the deformation gradient $\mathbf{F}$ as the linear map of material vectors from the reference state to the current state following the common practice in continuum mechanics [48].

3.2. Kinematic assumptions

A polymer jet is a 3D body. The accurate kinematics of the jet involves a 3D deformation field. A beam theory approximates the 3D deformation field with an asymptotic expansion around a 1D curve, the centerline. Here we expand the deformation gradient, $\mathbf{F}$, around the centerline of the jet as a power series with respect to the offset vector from the centerline, $\mathbf{h} = h_n\mathbf{n} + h_b\mathbf{b}$. We determine the expansion by the following three assumptions:

1. Deformation gradient is approximated to the first order in $\mathbf{h}$;
2. The cross-section normal and flat to the centerline remains normal and flat; and
3. The deformation in the $\mathbf{n}, \mathbf{b}$ plane is isotropic.

Assumption 1 implies a first order asymptotic theory. We use $O(h)$ to represent any term that is first order in $\mathbf{h}$, and $o(h)$ to represent any term that is higher order in $\mathbf{h}$. The theory is valid when $\mathbf{h}$ is small (i.e. the jet is thin) by some dimensionless criteria. As we will later identify, there are two criteria for a jet to be considered thin. The first requires the jet to be weakly bended or twisted $|\boldsymbol{\kappa} \times \mathbf{h}| \ll 1$. The second requires the stretch of the jet to be relatively homogeneous, $\partial\lambda/\partial s\,|\mathbf{h}| \ll 1$,where λ is the stretch of the material on the centerline relative to the reference state. The second criterion is required only when the deformation of the beam is dominated by twisting. Assumption 2 follows the classical Euler–Bernoulli beam theory. It approximate the rotation of a material cross-section by the rotation at the centerline. Assumption 3 specifies the in-plane deformation on the cross-section. Under common processing condition, the polymer jet can be treated as incompressible [49]. As we will later show, when the material incompressibility is enforced, the three assumptions completely determine the deformation gradient anywhere in the jet.

It is easier to work with the deformation gradient in the moving local frame than in the fixed lab frame. Introduce the decomposition

$$\mathbf{F} = \mathbf{R}\mathbf{F}^*. \tag{3.1}$$

Here $\mathbf{F}$ is the deformation gradient in the lab frame, $\mathbf{F}^*$ is the deformation gradient in the local frame. $\mathbf{R}$ is the rotation of the local frame relative to the lab frame. For the deformation gradient in the local frame, introduce the decomposition

$$\mathbf{F}^*(s, h_n, h_b, t) = \mathbf{H}(s, h_n, h_b, t)\,\mathbf{F}^*(s, 0, 0, t). \tag{3.2}$$

Here $\mathbf{F}^*(s, 0, 0, t)$ is the deformation gradient on the centerline. We call $\mathbf{H}$ the deformation gradient relative to the centerline. For the simplicity of notation, we use the following shorthand notation

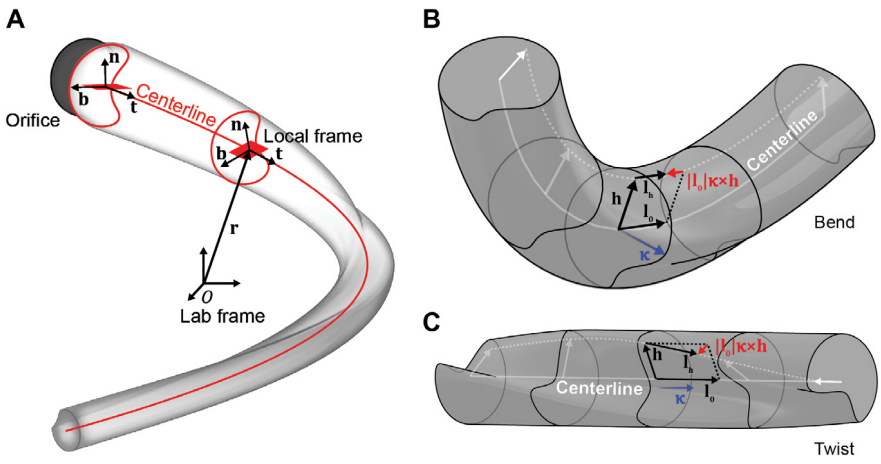

Fig. 1. **A**. The geometry of the jet is described by the centerline (red) which consists of all the material points that flow out from a fixed spatial point of the orifice. Consider a material surface tangent to the centerline (red). The normal vector of this material surface **n** marks the orientation of the jet. Together, the tangent vector of the centerline **t**, the normal vector **n**, and the vector $\mathbf{b} = \mathbf{t} \times \mathbf{n}$, define the local frame of reference for the jet. The relative offset between the moving local frame and the fixed lab frame is $\mathbf{r}(s)$, where s is the distance along the centerline from the orifice. **B**. the bending of the jet causes material lines to be compressed/stretched relative to the centerline. **C**. The twisting of the jet causes material lines to tilt relative to the centerline. (For interpretation of the references to color in this figure legend, the reader is referred to the web version of this article.)

$\mathbf{F}^*(\mathbf{h}) := \mathbf{F}^*(s, h_n, h_b, t)$. Following the three assumptions, $\mathbf{F}^*(0)$ must take the form

$$\mathbf{F}^*(0) = \begin{bmatrix} \lambda & & \\ & \frac{1}{\sqrt{\lambda}} & \\ & & \frac{1}{\sqrt{\lambda}} \end{bmatrix}. \tag{3.3}$$

Here λ is the stretch of the centerline with respect to the reference state. The jet contracts by $1/\sqrt{\lambda}$ in directions perpendicular to the centerline due to incompressibility.

Following the three assumptions **H** must take the form

$$\mathbf{H} = \begin{bmatrix} 1 + \boldsymbol{\kappa} \times \mathbf{h} \cdot \mathbf{t} & & \\ \boldsymbol{\kappa} \times \mathbf{h} \cdot \mathbf{n} & 1 - \frac{1}{2}\boldsymbol{\kappa} \times \mathbf{h} \cdot \mathbf{t} & \\ \boldsymbol{\kappa} \times \mathbf{h} \cdot \mathbf{b} & & 1 - \frac{1}{2}\boldsymbol{\kappa} \times \mathbf{h} \cdot \mathbf{t} \end{bmatrix} + o(h). \tag{3.4}$$

Consider two identical vectors parallel to **t** in the reference state, one on the centerline, $\mathbf{l}_0$, and the other offset by $\mathbf{h}, \mathbf{l}_\mathbf{h}$. In (3.4) $\boldsymbol{\kappa} \times \mathbf{h} \cdot \mathbf{t}$ describes the relative compression/stretching of $\mathbf{l}_\mathbf{h}$ relative to the $\mathbf{l}_0$ due to bending, Fig. 1B. The terms $\boldsymbol{\kappa} \times \mathbf{h} \cdot \mathbf{n}$ and $\boldsymbol{\kappa} \times \mathbf{h} \cdot \mathbf{b}$ describe the tilting of $\mathbf{l}_\mathbf{h}$ relative to $\mathbf{l}_0$ due to twisting, Fig. 1C. The first column can be obtained based on Assumption 2 in the same way as in the elementary beam theory [45]. The isotropic in plane expansion/contraction of the cross-section, $-\frac{1}{2}\boldsymbol{\kappa} \times \mathbf{h} \cdot \mathbf{t}$, follows from Assumption 3. It enforces material incompressibility to $O(h)$. Combining (3.2)–(3.4) we have the expression

$$\mathbf{F}^*(\mathbf{h}) = \begin{bmatrix} \lambda(1 + \boldsymbol{\kappa} \times \mathbf{h} \cdot \mathbf{t}) & & \\ \lambda\boldsymbol{\kappa} \times \mathbf{h} \cdot \mathbf{n} & \frac{1}{\sqrt{\lambda}}\left(1 - \frac{1}{2}\boldsymbol{\kappa} \times \mathbf{h} \cdot \mathbf{t}\right) & \\ \lambda\boldsymbol{\kappa} \times \mathbf{h} \cdot \mathbf{b} & & \frac{1}{\sqrt{\lambda}}\left(1 - \frac{1}{2}\boldsymbol{\kappa} \times \mathbf{h} \cdot \mathbf{t}\right) \end{bmatrix} + o(h). \tag{3.5}$$

Here $\mathbf{F}^*(\mathbf{h})$ is completely expressed in terms of the deformation of the centerline, λ, $\boldsymbol{\kappa}$, and the offset from the centerline **h**.

3.3. Choice of centerline

Assumptions 2 and 3 are specific to the choice of the centerline. One may then ask how the beam model differs if we choose a different centerline. In the supplementary materials Section 2, we show that the choice of centerline changes the model at $O(h^2)$ or higher order. Since our beam theory is asymptotic to the $O(h)$ order, it is independent of the choice of the centerline. For the asymptotic theory to be valid, we require the difference at $O(h^2)$ level caused by choosing a different centerline is negligible. This requirement gives our two criteria for a jet to be considered thin:

1. $|\boldsymbol{\kappa} \times \mathbf{h}| \ll 1$; and
2. $\partial\lambda/\partial s\,|\mathbf{h}| \ll 1$.

The first criterion implies weak bending or twisting. The second criterion implies nearly homogeneous stretching, where λ is the stretch of the material on the centerline. The second criterion is required only when the deformation of the beam is dominated by twisting.

3.4. Velocity gradient

Viscoelasticity is a rate dependent behavior. Rate of deformation is often described by the velocity gradient [48]. The velocity gradient is related to the deformation gradient by [48]

$$\mathbf{L} = \dot{\mathbf{F}}\mathbf{F}^{-1}. \tag{3.6}$$

Here a dot on top means the material derivative of the quantity. Using the expression of deformation gradient in the last section, we obtain the velocity gradient in the local frame as (supplementary materials Section 3)

$$\mathbf{L}^*(\mathbf{h}) = \mathbf{L}^*(0) + \delta\mathbf{L}^* + o(h). \tag{3.7}$$

Here $\mathbf{L}^*(0)$ is the $O(1)$ term and $\delta\mathbf{L}^*$ is the $O(h)$ term, with the expressions given in Box I. Here u is the velocity of the jet along the centerline. Eqs. (3.7)–(3.9) completely express $\mathbf{L}^*(\mathbf{h})$ in terms of geometric quantities of the centerline, $\partial u/\partial s$, $\boldsymbol{\kappa}$, $\boldsymbol{\omega}$, and the offset from the centerline **h**.

$$\mathbf{L}^*(0) = \begin{bmatrix} \frac{\partial u}{\partial s} & & \\ & -\frac{1}{2}\frac{\partial u}{\partial s} & \\ & & -\frac{1}{2}\frac{\partial u}{\partial s} \end{bmatrix}, \quad \text{and} \tag{3.8}$$

$$\delta\mathbf{L}^* = \begin{bmatrix} \left(\frac{D^*\boldsymbol{\kappa}}{Dt} - \frac{1}{2}\frac{\partial u}{\partial s}\boldsymbol{\kappa}\right)\times\mathbf{h}\cdot\mathbf{t} & & \\ \frac{\partial\boldsymbol{\omega}}{\partial s}\times\mathbf{h}\cdot\mathbf{n} & -\frac{1}{2}\left(\frac{D^*\boldsymbol{\kappa}}{Dt} - \frac{1}{2}\frac{\partial u}{\partial s}\boldsymbol{\kappa}\right)\times\mathbf{h}\cdot\mathbf{t} & \\ \frac{\partial\boldsymbol{\omega}}{\partial s}\times\mathbf{h}\cdot\mathbf{b} & & -\frac{1}{2}\left(\frac{D^*\boldsymbol{\kappa}}{Dt} - \frac{1}{2}\frac{\partial u}{\partial s}\boldsymbol{\kappa}\right)\times\mathbf{h}\cdot\mathbf{t} \end{bmatrix}. \tag{3.9}$$

Box I. .

4. Constitutive relation of a polymer jet

Section 3 expresses the deformation gradient $\mathbf{F}$ and the velocity gradient $\mathbf{L}$ anywhere in the jet based on the shape and motion of the centerline, $\mathbf{v}$, $\boldsymbol{\kappa}$, $\boldsymbol{\omega}$. The stress field in the jet can be calculated using any material model. Since the kinematics has an intrinsic error of $o(h)$, propagating the error through the material model, the stress field is expected to have an error of $o(h)$ as well. Once we have the stress field, the force and torque in the jet can be calculated. Here we demonstrate this procedure with the Oldroyd-B model [46,47].

4.1. Oldroyd-B viscoelastic model

Polymer jets are made of viscoelastic polymer solutions or melts. The deformation of the polymer jet can be decomposed into two parts, the viscous deformation and the elastic deformation. The viscous deformation corresponds to the sliding between polymer chains without changing the chain configuration. The elastic deformation corresponds to the stretching of the polymer chain while keeping the relative position of the polymer chains fixed, Fig. 2A. The deformation gradient can be decomposed into the viscous part and the elastic part correspondingly [50],

$$\mathbf{F} = \mathbf{F}_e\mathbf{F}_v. \tag{4.1}$$

An intermediate state is defined as the state where the elastic energy in the polymer chains in the current state is released [50], Fig. 2A.

Here we give an original formulation of Oldroyd-B model using the spring–dashpot diagram in Fig. 2B, with $\boldsymbol{\sigma}_e$, $\boldsymbol{\sigma}_v$, $\boldsymbol{\sigma}_s$ represent, respectively, the elastic stress due to polymer, the viscous stress due to polymer, and the viscous stress due to solvent. The elastic stress due to the stretching of polymer chains follows the Neo-Hookean model,

$$\boldsymbol{\sigma}_e = \mu(\mathbf{F}_e\mathbf{F}_e^T - \mathbf{I}). \tag{4.2}$$

Here μ is the shear modulus, and $\mathbf{I}$ is the identity matrix. The viscous stress due to polymer chains sliding apart has the expression

$$\boldsymbol{\sigma}_v = \zeta\mathbf{F}_e\left(\dot{\mathbf{F}}_v\mathbf{F}_v^{-1} + \mathbf{F}_v^{-T}\dot{\mathbf{F}}_v^T\right)\mathbf{F}_e^T. \tag{4.3}$$

Here ζ is a constant describing the sliding of the polymer chains. $\dot{\mathbf{F}}_v\mathbf{F}_v^{-1}$ is the velocity gradient in the intermediate state. Eq. (4.3) can be viewed as a pushforward of a linear viscous relation from the intermediate state to the current state. The viscous stress due to solvent molecules sliding apart follows the Newton's law of viscosity,

$$\boldsymbol{\sigma}_s = \eta\left(\dot{\mathbf{F}}\mathbf{F}^{-1} + \mathbf{F}^{-T}\dot{\mathbf{F}}^T\right). \tag{4.4}$$

Here η is the viscosity of the solvent.

According to Fig. 2B, we require

$$\boldsymbol{\sigma}_e = \boldsymbol{\sigma}_v. \tag{4.5}$$

We assumed that the polymer jet is incompressible. The total stress $\boldsymbol{\sigma}$ has the expression

$$\boldsymbol{\sigma} = \boldsymbol{\sigma}_e + \boldsymbol{\sigma}_s + p\mathbf{I} \tag{4.6}$$

Here p is a hydrostatic pressure applied on the material. (4.2)–(4.6) defines the Oldroyd-B model.

Oldroyd-B model is frame indifferent, so (4.2)–(4.6) take the same form in the local frame. Eqs. (4.2)–(4.6) can be simplified to two equations:

$$\mu\left(\mathbf{B}_e^* - \mathbf{I}\right) = -\zeta\left(\frac{D^*\mathbf{B}_e^*}{Dt} - \mathbf{L}^*\mathbf{B}_e^* - \mathbf{B}_e^*\mathbf{L}^{*T}\right), \tag{4.7}$$

$$\boldsymbol{\sigma}^* = \mu\left(\mathbf{B}_e^* - \mathbf{I}\right) + \eta\left(\mathbf{L}^* + \mathbf{L}^{*T}\right) + p\mathbf{I}. \tag{4.8}$$

Here $\mathbf{B}_e^* = \mathbf{F}_e^*\mathbf{F}_e^{*T}$ is the left Cauchy–Green tensor of the elastic deformation in the local frame. $D^*\mathbf{B}_e^*/Dt = \dot{\mathbf{B}}_e^* - \mathbf{W}\mathbf{B}_e^* + \mathbf{B}_e^*\mathbf{W}$. The right hand side of (4.7) is the upper-convected derivative of $\mathbf{B}_e$ [51], characterizing the changing rate of $\mathbf{B}_e$ in a frame following the moving and deforming of material. If we cancel out $\mathbf{B}_e$ from (4.7)–(4.8), we will reach the commonly used form of Oldroyd-B model in terms of the upper-convected derivative of stress (supplementary materials Section 4).

4.2. The beam model of an Oldroyd-B jet

We obtain the beam model by combining the kinematics in Section 3.4 and the Oldroyd-B model. Substitute the expression of $\mathbf{L}^*$ (3.7) into (4.7), one can verify that $\mathbf{B}_e^*$ also has an intrinsic error of $o(h)$. Expand $\mathbf{B}_e^*$ and we get

$$\mathbf{B}_e^*(\mathbf{h}) = \mathbf{B}_e^*(0) + \delta\mathbf{B}_e^*(\mathbf{h}) + o(h). \tag{4.9}$$

Here $\delta\mathbf{B}_e^*(\mathbf{h})$ represents the first order term. At the zeroth order, Oldroyd-B model (4.7) gives

$$\frac{D^*\mathbf{B}_e^*(0)}{Dt} - \mathbf{L}^*(0)\mathbf{B}_e^*(0) - \mathbf{B}_e^*(0)\mathbf{L}^{*T}(0) = -\frac{\mu}{\zeta}\left(\mathbf{B}_e^*(0) - \mathbf{I}\right). \tag{4.10}$$

Here the left-hand-side is the upper-convected derivative of $\mathbf{B}_e$ on the centerline. At the first order, (4.7) yields

$$\frac{D^*\delta\mathbf{B}_e^*}{Dt} - \mathbf{L}^*(0)\delta\mathbf{B}_e^* - \delta\mathbf{B}_e^*\mathbf{L}^{*T}(0) = -\frac{\mu}{\zeta}\delta\mathbf{B}_e^* + \delta\mathbf{L}\mathbf{B}_e^*(0) + \mathbf{B}_e^*(0)\delta\mathbf{L}^T. \tag{4.11}$$

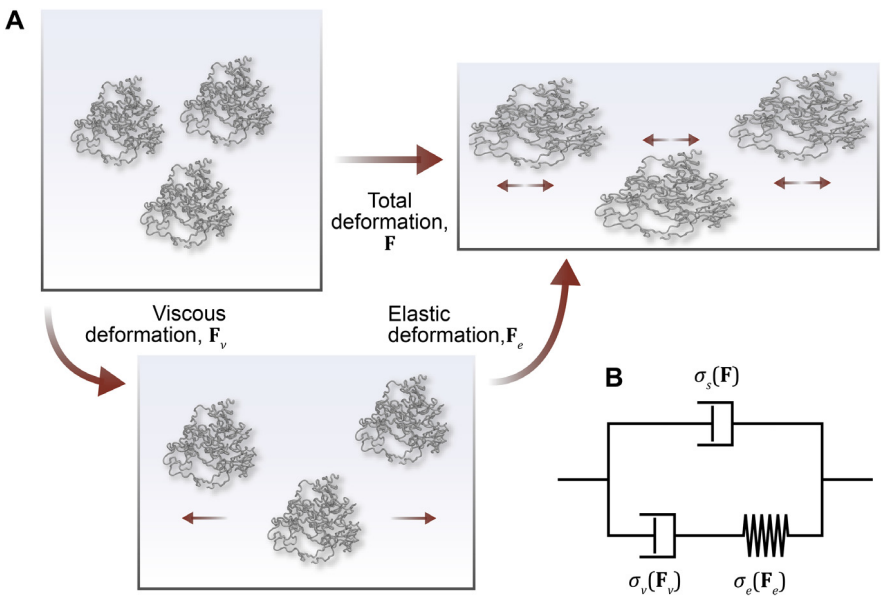

Fig. 2. A. The deformation of a polymer melt or polymer solution can be decomposed into the viscous part and the elastic part. The viscous part consists of the relative sliding between neighboring polymer chains without deforming the chains. The elastic part consists of stretching the polymer chains while keeping the relative positions of the chains fixed. **B**. Representation of the Oldroyd-B model in a spring–dashpot diagram.

Here the left-hand-side is not an upper-convected derivative since $\mathbf{L}^*(0)$ is evaluated on the centerline but $\delta\mathbf{B}_e^*$ is generally offset from the centerline.

In general, matrix Eqs. (4.10)–(4.11) are twelve independent equations for the six components of $\mathbf{B}_e^*(0)$ and the six components of $\delta\mathbf{B}_e^*$. In practice, material only has finite memory of its loading history. When all the memory of the reference state is forgotten, $\mathbf{B}_e^*(0)$ and $\delta\mathbf{B}_e^*$ take the following forms:

$$\mathbf{B}_e^*(0) = \begin{bmatrix} \lambda_{e\parallel}^2 & & \\ & \lambda_{e\perp}^2 & \\ & & \lambda_{e\perp}^2 \end{bmatrix}, \tag{4.12}$$

$$\delta\mathbf{B}_e^*(\mathbf{h}) = \begin{bmatrix} \boldsymbol{\beta}\times\mathbf{h}\cdot\mathbf{t} & \boldsymbol{\beta}\times\mathbf{h}\cdot\mathbf{n} & \boldsymbol{\beta}\times\mathbf{h}\cdot\mathbf{b} \\ \boldsymbol{\beta}\times\mathbf{h}\cdot\mathbf{n} & \chi\boldsymbol{\beta}\times\mathbf{h}\cdot\mathbf{t} & \\ \boldsymbol{\beta}\times\mathbf{h}\cdot\mathbf{b} & & \chi\boldsymbol{\beta}\times\mathbf{h}\cdot\mathbf{t} \end{bmatrix}. \tag{4.13}$$

Here $\lambda_{e\parallel}^2$, $\lambda_{e\perp}^2$, $\boldsymbol{\beta}$, χ are unknowns. $\lambda_{e\parallel}$ and $\lambda_{e\perp}$ are the stretch of the polymer chain in the direction parallel to the centerline and perpendicular to the centerline. Note that the stretch of the polymer chain is generally different from the stretch of the jet due to the presence of viscous relaxation. $\boldsymbol{\beta}$, χ characterize the gradient of the stretch of the polymer chains across the cross-section. In this case, (4.10) consists of two equations for $\lambda_{e\parallel}^2$, $\lambda_{e\perp}^2$ and (4.11) consists of four equations for the vector $\boldsymbol{\beta}$ and the scalar χ. Eqs. (4.10)–(4.11) can be solved given the material parameters μ, ζ and the geometric quantities of the centerline, $\partial u/\partial s$, $\boldsymbol{\kappa}$, $\boldsymbol{\omega}$. We assume (4.12) and (4.13) to be true for the rest of the discussion.

As $\mathbf{B}_e^*(\mathbf{h})$ is determined through (4.9), (4.12)–(4.13) to $O(h)$, stress can be determined by the Oldroyd-B model (4.8) to $O(h)$, with an unknown hydrostatic pressure, p. To determine the hydrostatic pressure, we assume that the surface of the jet is stress-free, which implies $\sigma_{\mathrm{nn}} = \sigma_{\mathrm{bb}} = 0$. Consequently

$$p = \eta\frac{\partial u}{\partial s} - \mu\left(\lambda_{e\perp}^2 - 1\right) + \left(\eta\left(\frac{D^*\boldsymbol{\kappa}}{Dt} - \frac{1}{2}\frac{\partial u}{\partial s}\boldsymbol{\kappa}\right) - \mu\chi\boldsymbol{\beta}\right) \times \mathbf{h}\cdot\mathbf{t} + o(h). \tag{4.14}$$

The traction on a cross-section normal to the centerline can now be calculated. We get

$$\boldsymbol{\sigma t} = \left[\ \mu\left(\lambda_{e\parallel}^2 - \lambda_{e\perp}^2\right) + 3\eta\tfrac{\partial u}{\partial s}\ \right] + \begin{bmatrix} \mathbf{m}_{bend}\times\mathbf{h}\cdot\mathbf{t} \\ \mathbf{m}_{twist}\times\mathbf{h}\cdot\mathbf{n} \\ \mathbf{m}_{twist}\times\mathbf{h}\cdot\mathbf{b} \end{bmatrix} + o(h), \tag{4.15}$$

with $\mathbf{m}_{bend} = \mu(1-\chi)\boldsymbol{\beta} + 3\eta\left(\frac{D^*\boldsymbol{\kappa}}{Dt} - \frac{1}{2}\frac{\partial u}{\partial s}\boldsymbol{\kappa}\right)$ and $\mathbf{m}_{twist} = \mu\boldsymbol{\beta} + \eta\frac{\partial\boldsymbol{\omega}}{\partial s}$.

The traction (4.15) can be integrated to obtain the total force and torque in the jet. Here it is convenient to locate the centerline at the centroid of the cross-section so that the integration of odd order terms of $\mathbf{h}$ cancels out. The total force and torque on the cross-section can be integrated by $\mathbf{f} = \int_A \boldsymbol{\sigma t}\,\mathrm{d}a$ and $\mathbf{M} = \int_A \mathbf{h}\times(\boldsymbol{\sigma t})\,\mathrm{d}a$. Here A is the cross-section area normal to the centerline. As discussed in Section 3.3, the choice of the centerline is arbitrary, we locate the centerline at the centroid of the cross-section so that the integration of odd order terms of $\mathbf{h}$ cancels out.

$$\mathbf{f} = \left(\mu A\left(\lambda_{e\parallel}^2 - \lambda_{e\perp}^2\right) + 3\eta A\frac{\partial u}{\partial s}\right)\mathbf{t} + o\left(h^3\right). \tag{4.16}$$

$$\mathbf{M} = \begin{bmatrix} J_{tt} & & \\ & J_{nn} & J_{nb} \\ & J_{nb} & J_{bb} \end{bmatrix}\begin{bmatrix} \mathbf{m}_{twist}\cdot\mathbf{t} \\ \mathbf{m}_{bend}\cdot\mathbf{n} \\ \mathbf{m}_{bend}\cdot\mathbf{b} \end{bmatrix} + o\left(h^4\right). \tag{4.17}$$

Here $J_{tt} = \int_A \mathbf{h}\cdot\mathbf{h}\mathrm{d}a$, $J_{nn} = \int_A(\mathbf{h}\cdot\mathbf{b})^2\,\mathrm{d}a$, $J_{bb} = \int_A(\mathbf{h}\cdot\mathbf{n})^2\,\mathrm{d}a$, and $J_{nb} = -\int_A(\mathbf{h}\cdot\mathbf{n})(\mathbf{h}\cdot\mathbf{b})\,\mathrm{d}a$ constitutes the tensor of the second moment of area of the cross-section.

5. Conservation laws

Take a control volume bounded by the surface of the jet and two cross-sections normal to the centerline located at s and s'. The conservation of mass requires

$$\frac{\partial}{\partial t}\int_V \rho\mathrm{d}V + \int_{A(s')}(\mathbf{v}\cdot\mathbf{t})\,\rho\mathrm{d}A - \int_{A(s)}(\mathbf{v}\cdot\mathbf{t})\,\rho\mathrm{d}A = \int_s^{s'}\dot{m}\mathrm{d}s. \tag{5.1}$$

Here ρ is the density of the material. $\dot{m}$ is the mass exchange per unit length of the jet, e.g. through the evaporation of the solvent.

Integrate over the cross-section using the velocity distribution (S3.10), we get the differential equation

$$\frac{\partial(\rho A)}{\partial t}+\frac{\partial}{\partial s}(u\rho A)=\dot{m}. \tag{5.2}$$

The conservation of momentum requires

$$\begin{aligned}&\frac{\partial}{\partial t}\int_V \rho\mathbf{v}\mathrm{d}V+\int_{A(s')}(\mathbf{v}\cdot\mathbf{t})\,\rho\mathbf{v}\mathrm{d}A-\int_{A(s)}(\mathbf{v}\cdot\mathbf{t})\,\rho\mathbf{v}\mathrm{d}A\\&=\mathbf{f}(s')-\mathbf{f}(s)+\int_V\mathbf{q}\mathrm{d}V.\end{aligned} \tag{5.3}$$

Here $\mathbf{q}$ is the body forces, such as gravity, centrifugal force and Coriolis force. Locate the centerline locates at the centroid, the integration of any first order terms over the cross-section vanishes, we have

$$\frac{\partial}{\partial t}(\rho A\mathbf{v})+\frac{\partial}{\partial s}(u\rho A\mathbf{v})=\frac{\partial\mathbf{f}}{\partial s}+A\mathbf{q}. \tag{5.4}$$

The conservation of angular momentum requires

$$\begin{aligned}&\frac{\partial}{\partial t}\int_V(\mathbf{r}+\mathbf{h})\times\rho\mathbf{v}\mathrm{d}V+\int_{A(s')}(\mathbf{v}\cdot\mathbf{t})\,(\mathbf{r}+\mathbf{h})\times\rho\mathbf{v}\mathrm{d}A\\&-\int_{A(s)}(\mathbf{v}\cdot\mathbf{t})\,(\mathbf{r}+\mathbf{h})\times\rho\mathbf{v}\mathrm{d}A\\&=\int_{A(s')}(\mathbf{r}+\mathbf{h})\times\boldsymbol{\sigma}\mathbf{t}\mathrm{d}A-\int_{A(s)}(\mathbf{r}+\mathbf{h})\times\boldsymbol{\sigma}\mathbf{t}\mathrm{d}A\\&+\int_V(\mathbf{r}+\mathbf{h})\times\mathbf{q}\mathrm{d}V.\end{aligned} \tag{5.5}$$

Locate the centerline at the centroid, the integration of any first order terms over the cross-section vanishes, we get

$$\frac{\partial}{\partial t}(\mathbf{r}\times\rho A\mathbf{v})+\frac{\partial}{\partial s}(\mathbf{r}\times u\rho A\mathbf{v})=\mathbf{r}\times\frac{\partial\mathbf{f}}{\partial s}+\mathbf{t}\times\mathbf{f}+\frac{\partial\mathbf{M}}{\partial s}+\mathbf{r}\times A\mathbf{q}. \tag{5.6}$$

Use (5.4) to cancel out the dependence on the absolute position $\mathbf{r}$, we get

$$\frac{\partial}{\partial t}(\rho\mathbf{J}!)+\frac{\partial}{\partial s}(2u\rho\mathbf{J}!-\mathbf{t}(\mathbf{v}\cdot\rho\mathbf{J}!))=\mathbf{t}\times\mathbf{f}+\frac{\partial\mathbf{M}}{\partial s}. \tag{5.7}$$

Note that $\mathbf{J}\sim O(h^4)$, so that $\mathbf{t}\times\mathbf{f}$ is $O(h^4)$. This is a higher order term that is not predicted by the material model (4.16).

6. Rotary jet spinning

Rotary jet spinning is a platform that uses centrifugal force to produce nanofiber. It is praised for its orders-of-magnitude improvement in production rate comparing to conventional electrospinning [11]. Rotary jet spinning consists of a rapidly rotating reservoir where polymer solution/polymer melt is fed in [9,10], Fig. 3. A few orifices are opened on the side of the reservoir. Under the centrifugal force, the polymer solution is pulled out from an orifice and form a polymer jet. The polymer jet is elongated and bended under centrifugal force, Coriolis force, air drag, and gravity. The elongated polymer jet then solidifies by the evaporation of the solvent [9], cooling below the melting temperature [14], or entering a precipitation bath [13]. Previous studies show that the jet may be acutely bended near the orifice due to a combination of centrifugal force, Coriolis force, and viscous stress, where a string model fails to model rotary jet spinning [31]. While the existing beam model of rotary jet spinning resolves the bending near the orifice, it only studies viscous jet with no viscoelastic relaxation [32]. In this section, we use the beam model developed in previous sections to model the fiber formation in rotary jet spinning.

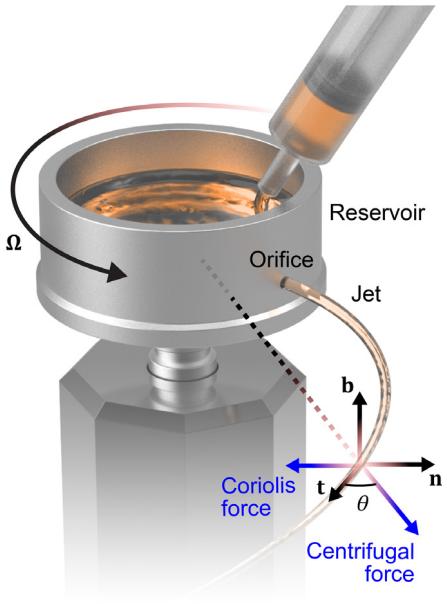

Fig. 3. Rotary jet spinning consists of a fast-rotating reservoir with an orifice opened on the side of the reservoir. The reservoir is fed with polymer dope from the top. During spinning, polymer jet is ejected from the orifice under centrifugal force. When gravity is neglected, the trajectory of the jet is confined in the $\mathbf{n}$, $\mathbf{t}$ plane in the figure.

For simplicity, we only model the steady state of a jet in rotary jet spinning. Gravity, air-drag, solvent evaporation, and solidification of the jet are neglected. Under these assumptions, a boundary value problem is formulated using the result derived in the previous sections (supplementary materials 5). The problem is governed by five dimensionless groups: the Reynolds number $Re=\rho v_0 r_0/\zeta$ characterizing the competition between inertia and the viscoelasticity in the jet, the Rossby number $Ro=v_0/\Omega r_0$ characterizing the effect of centrifugal force and Coriolis force, the Weissenberg number for the polymer part and the solvent part $Wi_p=\zeta v_0/\mu r_0$ and $Wi_s=\eta v_0/\mu r_0$, characterizing the viscoelastic relaxation in the jet, and the slenderness ratio $Sl=a_0/r_0$, comparing the resistance to the bending of the jet versus the resistant to the stretching of the jet.

In Fig. 4, we choose our simulation condition to represent common spinning condition by fixing $Re=1$, $Ro=0.1$, $Wi_s=10^{-2}$, $Sl=10^{-2}$ [4], and study the effect of the viscoelasticity of the polymer jet by varying $Wi_p=0.01, 0.1, 1$. When $Wi_p=0.01$, the viscoelastic relaxation is fast comparing to the time scale of deforming. The jet behaves like a viscous fluid. When $Wi_p=1$, the viscoelastic relaxation and the time scale of deforming is comparable. The jet behaves like an elastic solid near the reservoir.

Fig. 4A plots the trajectories of the jets of different Wi_p. As the jet become more elastic, the jet goes closer around the reservoir. In fact, a perfectly elastic jet would fall onto a fast rotating reservoir with $Ro<1$ (supplementary material Section 6). Fig. 4B compares the fiber radius. The highly viscous jet ($Wi_p=0.01$) experiences constant reduction in radius during the spinning, as the centrifugal force keeps driving the viscous thinning of the jet. On the other hand, the highly elastic jet ($Wi_p=1$) resists reduction in radius in most range of the jet ($10^{-1}<s/r_0<10^{1}$), after an abrupt strongly stretched near the orifice ($s/r_0<10^{-1}$). This is because that the elasticity can withstand a constant stress without thinning out. The localized stretch is where the elastic deformation happens. In Fig. 4C, we plot the stretch of polymer chains: $\lambda_{chain}=\sqrt{(\lambda_{e\|}^2+2\lambda_{e\perp}^2)/3}$ [52]. The stretch of polymer chains is an indicator

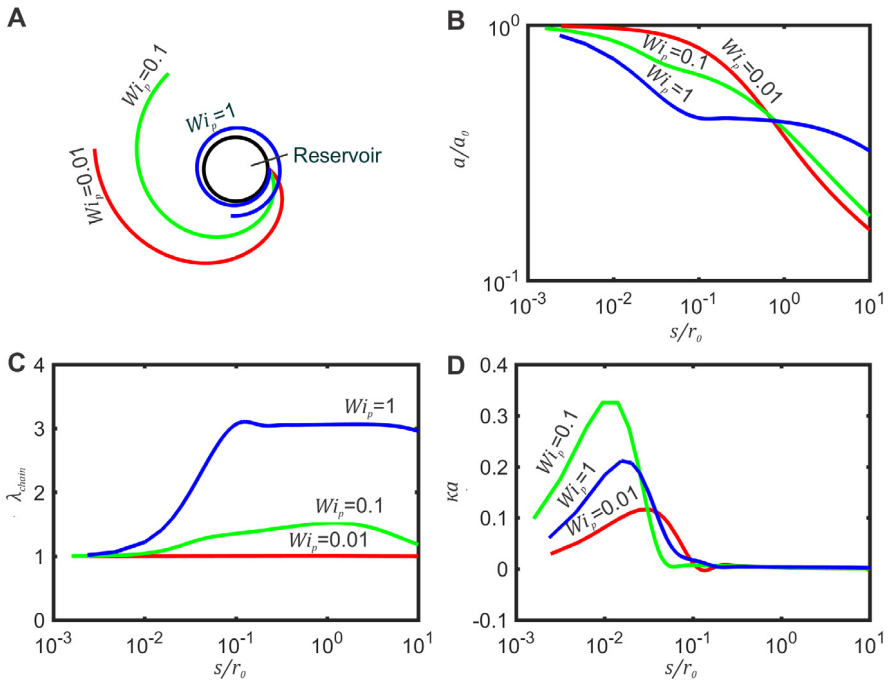

Fig. 4. **A**. The trajectory of the jet shows that the more elastic jet (higher Wi_p) wraps closer around the reservoir. **B.** The radius of the jet a normalized by the radius of the orifice a_0 shows that the more viscous jet ($Wi_p = 0.01$) keeps thinning under centrifugal force while the more elastic jet ($Wi_p = 1$) resists the thinning after a finite deformation near the orifice. **C.** The stretch of the polymer chain λ_{chain} shows that spinning viscous jet ($Wi_p = 0.01$) does not align polymer chains while spinning elastic jet ($Wi_p = 1$) accumulates chain alignment. **D.** The curvature normalized by the radius of the jet show that bending deformation localizes at a small region near the orifice. The result is also consistent with the criterion of thin jet $|\boldsymbol{\kappa} \times \mathbf{h}| \ll 1$.

of the microscopic chain alignment, which is desirable in creating ultra-strong fibers [53] or inducing certain protein folding [54]. Fig. 4C shows that viscous jet ($Wi_p = 0.01$) does not induce any chain stretch as the viscoelastic relaxation is too fast comparing to the deformation rate. In contrast, the elastic jet ($Wi_p = 1$) accumulates chain stretch. In the intermediate case ($Wi_p = 0.1$), polymer chains are stretched initially ($s/r_0 < 10^0$) when the deformation is rapid. The chain stretch is gradually lost as the jet flies further away from the reservoir ($s/r_0 > 10^0$) when the deformation rate drops. To probe how the beam bending contributes to the deformation of the jet, we plot the curvature normalized by the jet radius along the jet in Fig. 4D. It shows that strong bending deformation localizes at a small region near the orifice, $s/r_0 < 0.1$. While the jet also has a finite curvature elsewhere as shown in Fig. 4A, the bending deformation is negligible due to the great reduction in the jet radius (see Fig. 4B). To make sure that the model is valid, we need to satisfy the criteria $|\boldsymbol{\kappa} \times \mathbf{h}| \ll 1$ and $\partial\lambda/\partial s\,|\mathbf{h}| \ll 1$. Since our jet is free of twisting, the second criterion is dropped. Fig. 4D show that $|\boldsymbol{\kappa} \times \mathbf{h}| \ll 1$ is indeed satisfied.

In summary, these simulations show that viscoelasticity strongly influence the rotary jet spinning process. The more elastic jet is better at align polymer chains but is poorer in reducing the fiber diameter, while the more viscous jet is the converse. It is important to design the spinning condition to achieve intermediate viscoelastic relaxation so that small fiber diameter and polymer chain alignment are achieved at the same time.

7. Conclusion remarks

This paper formulates a first-order beam theory for nonlinear viscoelastic material. The theory generalizes the classical Euler–Bernoulli theory to account for finite deformation and material incompressibility. The kinematics derived is then combined with the Oldroyd-B model to derive the constitutive equations of a nonlinear viscoelastic beam. The beam model is then used to study the viscoelastic relaxation in rotary jet spinning. Our model successfully captures the strong bending near the orifice that fails string models and the highly elastic behavior of the jet that cannot be modeled by existing beam model. Our theory has potential applications in many other manufacturing processes involving polymer jets, such as 3D printing, electro-spinning, and blow spinning.

Acknowledgments

This work was sponsored by the Wyss Institute for Biologically Inspired Engineering at Harvard University, and Harvard Materials Research Science and Engineering Center (MRSEC), United States grant DMR-1420570. We thank Michael Rosnach for assistance with photography and illustrations. The authors gratefully acknowledge the helpful feedback from Professor Zhigang Suo at Harvard University.

Appendix A. Supplementary data

Supplementary material related to this article can be found online at https://doi.org/10.1016/j.eml.2018.10.005.

References

[1] D.G. Baird, D.I. Collias, Polymer Processing: Principles and Design, John Wiley & Sons, 2014.
[2] T. Takajima, K. Kajiwara, J.E. McIntyre, Advanced Fiber Spinning Technology, Woodhead Publishing, 1994.
[3] A.L. Yarin, B. Pourdeyhimi, S. Ramakrishna, Fundamentals and Applications of Micro-And Nanofibers, Cambridge University Press, 2014.
[4] B. Mueller, Additive manufacturing technologies–Rapid prototyping to direct digital manufacturing, Assem. Autom. 32 (2) (2012).
[5] Z.-M. Huang, et al., A review on polymer nanofibers by electrospinning and their applications in nanocomposites, Compos. Sci. Technol. 63 (15) (2003) 2223–2253.
[6] A. Greiner, J.H. Wendorff, Electrospinning: A fascinating method for the preparation of ultrathin fibers, Angew. Chemie Int. Ed. 46 (30) (2007) 5670–5703.

[7] R. Butin, J. Keller, J. Harding, Non-Woven Mats by Melt Blowing, Google Patents, 1974.
[8] E.S. Medeiros, et al., Solution blow spinning: A new method to produce micro- and nanofibers from polymer solutions, J. Appl. Polymer Sci. 113 (4) (2009) 2322–2330.
[9] M.R. Badrossamay, et al., Nanofiber assembly by rotary jet-spinning, Nano Lett. 10 (6) (2010) 2257–2261.
[10] K. Sarkar, et al., Electrospinning to forcespinning™, Mater. Today 13 (11) (2010) 12–14.
[11] J.J. Rogalski, C.W. Bastiaansen, T. Peijs, Rotary jet spinning review–a potential high yield future for polymer nanofibers, Nanocomposites 3 (4) (2017) 97–121.
[12] M.R. Badrossamay, et al., Engineering hybrid polymer-protein super-aligned nanofibers via rotary jet spinning, Biomaterials 35 (10) (2014) 3188–3197.
[13] G.M. Gonzalez, et al., Production of synthetic, para-aramid and biopolymer nanofibers by immersion rotary jet-spinning, Macromol. Mater. Eng. 302 (1) (2017).
[14] Z. Xu, et al., Making nonwoven fibrous poly (ε caprolactone) constructs for antimicrobial and tissue engineering applications by pressurized melt gyration, Macromol. Mater. Eng. 301 (8) (2016) 922–934.
[15] H. Yuk, X. Zhao, A new 3D printing strategy by harnessing deformation, instability, and fracture of viscoelastic inks, Adv. Mater. 30 (6) (2018) 1704028.
[16] D. Li, Y. Xia, Electrospinning of nanofibers: Reinventing the wheel? Adv. Mater. 16 (14) (2004) 1151–1170.
[17] S. Sinha-Ray, A.L. Yarin, B. Pourdeyhimi, Meltblowing: I-basic physical mechanisms and threadline model, J. Appl. Phys. 108 (3) (2010) 034912.
[18] A.L. Yarin, S. Sinha-Ray, B. Pourdeyhimi, Meltblowing: II-linear and nonlinear waves on viscoelastic polymer jets, J. Appl. Phys. 108 (3) (2010) 034913.
[19] M.J. Divvela, et al., Discretized modeling for centrifugal spinning of viscoelastic liquids, J. Non-Newtonian Fluid Mech. 247 (2017) 62–77.
[20] D.H. Reneker, et al., Bending instability of electrically charged liquid jets of polymer solutions in electrospinning, J. Appl. Phys. 87 (9) (2000) 4531–4547.
[21] A.L. Yarin, S. Koombhongse, D.H. Reneker, Bending instability in electrospinning of nanofibers, J. Appl. Phys. 89 (5) (2001) 3018–3026.
[22] G.C. Rutledge, S.V. Fridrikh, Formation of fibers by electrospinning, Adv Drug Deliv Rev 59 (14) (2007) 1384–1391.
[23] R.S. Rao, R.L. Shambaugh, Vibration and stability in the melt blowing process, Ind. Eng. Chem. Res. 32 (12) (1993) 3100–3111.
[24] V.T. Marla, R.L. Shambaugh, Three-dimensional model of the melt-blowing process, Ind. Eng. Chem. Res. 42 (26) (2003) 6993–7005.
[25] S. Panda, N. Marheineke, R. Wegener, Systematic derivation of an asymptotic model for the dynamics of curved viscous fibers, Math. Methods Appl. Sci. 31 (10) (2008) 1153–1173.
[26] A. Hlod, Curved Jets of Viscous Fluid: Interactions with a Moving Wall, 2009.
[27] N. Marheineke, et al., Asymptotics and numerics for the upper-convected Maxwell model describing transient curved viscoelastic jets, Math. Models Methods Appl. Sci. 26 (03) (2016) 569–600.
[28] S. Chiu-Webster, J. Lister, The fall of a viscous thread onto a moving surface: A fluid-mechanical sewing machine, J. Fluid Mech. 569 (2006) 89–111.
[29] N.M. Ribe, M. Habibi, D. Bonn, Liquid rope coiling, Annu. Rev. Fluid Mech. 44 (2012) 249–266.
[30] T. Han, D.H. Reneker, A.L. Yarin, Buckling of jets in electrospinning, Polymer 48 (20) (2007) 6064–6076.
[31] T. Goetz, et al., Numerical evidence for the non-existence of stationary solutions of the equations describing rotational fiber spinning, Math. Models Methods Appl. Sci. 18 (10) (2008) 1829–1844.
[32] W. Arne, et al., Numerical analysis of cosserat rod and string models for viscous jets in rotational spinning processes, Math. Models Methods Appl. Sci. 20 (10) (2010) 1941–1965.
[33] S. Taghavi, R. Larson, Regularized thin-fiber model for nanofiber formation by centrifugal spinning, Phys. Rev. E 89 (2) (2014) 023011.
[34] S. Noroozi, et al., Regularized string model for nanofibre formation in centrifugal spinning methods, J. Fluid Mech. 822 (2017) 202–234.
[35] N.M. Ribe, J.R. Lister, S. Chiu-Webster, Stability of a dragged viscous thread: Onset of stitching in a fluid-mechanical sewing machine, Phys. Rev. 18 (12) (2006) 124105.
[36] W. Arne, N. Marheineke, R. Wegener, Asymptotic transition from cosserat rod to string models for curved viscous inertial jets, Math. Models Methods Appl. Sci. 21 (10) (2011) 1987–2018.
[37] M.K. Jawed, et al., Coiling of elastic rods on rigid substrates, Proc. Natl. Acad. Sci. 111 (41) (2014) 14663–14668.
[38] M.K. Jawed, P.-T. Brun, P.M. Reis, A geometric model for the coiling of an elastic rod deployed onto a moving substrate, J. Appl. Mech. 82 (12) (2015) 121007.
[39] J.C. Simo, J.E. Marsden, P.S. Krishnaprasad, The Hamiltonian structure of nonlinear elasticity: The material and convective representations of solids, rods, and plates, Arch. Ration. Mech. Anal. 104 (2) (1988) 125–183.
[40] J.C. Simo, A finite strain beam formulation. The three-dimensional dynamic problem. Part I, Comput. Methods Appl. Mech. Engrg. 49 (1) (1985) 55–70.
[41] J.C. Simo, L. Vu-Quoc, A geometrically-exact rod model incorporating shear and torsion-warping deformation, Int. J. Solids Struct. 27 (3) (1991) 371–393.
[42] H. Lang, J. Linn, M. Arnold, Multi-body dynamics simulation of geometrically exact cosserat rods, Multibody Syst. Dyn. 25 (3) (2011) 285–312.
[43] J. Linn, H. Lang, A. Tuganov, Geometrically exact Cosserat rods with Kelvin–Voigt type viscous damping, Mech. Sci. 4 (1) (2013) 79–96.
[44] Y. Liu, Z.-J. You, S.-Z. Gao, A continuous 1-D model for the coiling of a weakly viscoelastic jet, Acta Mech. (2017) 1–14.
[45] J. Gere, S. Timoshenko, Mechanics of materials, 1997, PWS-KENT Publishing Company, 1997, ISBN 0, 534 (92174) p.4.
[46] J. Oldroyd, On the formulation of rheological equations of state, Proc. R. Soc. Lond. Ser. A Math. Phys. Eng. Sci. 200 (1063) (1950) 523–541.
[47] R.G. Larson, The Structure and Rheology of Complex Fluids 150, Oxford university press New York, 1999.
[48] M.E. Gurtin, E. Fried, L. Anand, The Mechanics and Thermodynamics of Continua, Cambridge University Press, 2010.
[49] R.G. Larson, Constitutive Equations for Polymer Melts and Solutions: Butterworths Series in Chemical Engineering, Butterworth-Heinemann, 2013.
[50] K. Rajagopal, A. Srinivasa, A thermodynamic frame work for rate type fluid models, J. Non-Newtonian Fluid Mech. 88 (3) (2000) 207–227.
[51] F. Irgens, Continuum Mechanics, Springer Science & Business Media, 2008.
[52] E.M. Arruda, M.C. Boyce, A three-dimensional constitutive model for the large stretch behavior of rubber elastic materials, J. Mech. Phys. Solids 41 (2) (1993) 389–412.
[53] J.H. Park, G.C. Rutledge, 50th anniversary perspective: Advanced polymer fibers: High performance and ultrafine, Macromolecules 50 (15) (2017) 5627–5642.
[54] C.O. Chantre, et al., Production-scale fibronectin nanofibers promote wound closure and tissue repair in a dermal mouse model, Biomaterials 166 (2018) 96–108.

Supplementary materials

1. Kinematic relations

$\mathbf{t}$ and $\mathbf{v}$, or $\boldsymbol{\kappa}$ and $\boldsymbol{\omega}$ are kinematically related. Denote the axial velocity as $u = \mathbf{v} \cdot \mathbf{t}$. The material derivative has the expression

$$\frac{D}{Dt} = \frac{\partial}{\partial t} + u\frac{\partial}{\partial s}. \quad \text{(S1.1)}$$

Exchange the sequence of taking $\partial/\partial t$ and $\partial/\partial s$ in (2.1-2.4), we have:

$$\frac{\partial \mathbf{v}}{\partial s} = \frac{\partial u}{\partial s}\mathbf{t} + \boldsymbol{\omega} \times \mathbf{t}, \quad \text{(S1.2)}$$

$$\frac{\partial \boldsymbol{\omega}}{\partial s} = \frac{\partial u}{\partial s}\boldsymbol{\kappa} + \frac{D\boldsymbol{\kappa}}{Dt} - \boldsymbol{\omega} \times \boldsymbol{\kappa}. \quad \text{(S1.3)}$$

Equation (S1.2) says that the velocity gradient along the centerline consists of two parts: the acceleration along the jet ($\partial u/\partial s\,\mathbf{t}$) and the rotation of the material ($\boldsymbol{\omega} \times \mathbf{t}$). Equation (S1.3) says that the gradient of the angular velocity along the centerline consists of two parts: acceleration while traveling through a bend ($\partial u/\partial s\,\boldsymbol{\kappa}$) and bending of the material element ($D\boldsymbol{\kappa}/Dt - \boldsymbol{\omega} \times \boldsymbol{\kappa}$). At steady state, $\partial/\partial t = 0$.We have $\mathbf{t}$ and $\mathbf{v}$ in the same direction, so are $\boldsymbol{\kappa}$ and $\boldsymbol{\omega}$. Equations (S1.2-S1.3) are replaced by the simple relations:

$$\mathbf{v} = u\mathbf{t}. \quad \text{(S1.4)}$$

$$\boldsymbol{\omega} = u\boldsymbol{\kappa}. \quad \text{(S1.5)}$$

2. Choice of centerline

Imagine a centerline that is shifted by $\mathbf{d}\sim O(h)$ from the original centerline in the $\mathbf{n}, \mathbf{b}$ plane. We can formulate a new beam theory using the new centerline based on our assumptions. According to the original theory, the deformation gradient at the new centerline $\mathbf{0}' = \mathbf{d} + \mathbf{0}$ is, using (3.5),

$$\mathbf{F}^*(\mathbf{0}') = \begin{bmatrix} \lambda(1+\boldsymbol{\kappa}\times\mathbf{d}\cdot\mathbf{t}) & & \\ \frac{1}{\sqrt{\lambda}}\boldsymbol{\kappa}\times\mathbf{d}\cdot\mathbf{n} & \frac{1}{\sqrt{\lambda}}\left(1-\frac{1}{2}\boldsymbol{\kappa}\times\mathbf{d}\cdot\mathbf{t}\right) & \\ \frac{1}{\sqrt{\lambda}}\boldsymbol{\kappa}\times\mathbf{d}\cdot\mathbf{b} & & \frac{1}{\sqrt{\lambda}}\left(1-\frac{1}{2}\boldsymbol{\kappa}\times\mathbf{d}\cdot\mathbf{t}\right) \end{bmatrix} + o(h). \tag{S2.1}$$

Note that the first column is a vector tangent to the new centerline. The $\frac{1}{\sqrt{\lambda}}\boldsymbol{\kappa}\times\mathbf{d}\cdot\mathbf{n}$ and $\frac{1}{\sqrt{\lambda}}\boldsymbol{\kappa}\times\mathbf{d}\cdot\mathbf{b}$ terms indicate the tilting of the new centerline relative to the original cross-section. The new $\mathbf{n}, \mathbf{b}$ cross-section is also tilted relative to the original cross-section. Consider an offset $\mathbf{h}'$ in the new cross-section, we have the transformation, Fig.S1,

$$\mathbf{h}' = \mathbf{h} - \mathbf{d} - \frac{1}{\lambda^{3/2}}\frac{\boldsymbol{\kappa}\times\mathbf{d}\cdot\mathbf{h}}{1+\boldsymbol{\kappa}\times\mathbf{d}\cdot\mathbf{t}}\mathbf{t}. \tag{S2.2}$$

Here $\mathbf{h}$ represents the offset in the original cross-section. The last term is a shift along the original centerline. Denote the deformation gradient in the new theory as $\mathbf{F}'(\mathbf{h}')$. Using the original theory, we have

$$\mathbf{F}'(\mathbf{h}') = \mathbf{F}^*(\mathbf{h}) - \int_{s_0}^{s_1}\frac{\partial\mathbf{F}^*(\mathbf{h})}{\partial s}ds + o(h) \tag{S2.3}$$

Here s_0 is the location of the original cross-section on the centerline. $s_1 = s_0 - \frac{1}{\lambda^{3/2}}\frac{\boldsymbol{\kappa}\times\mathbf{d}\cdot\mathbf{h}}{1+\boldsymbol{\kappa}\times\mathbf{d}\cdot\mathbf{t}}$. To the $O(h)$ order we have

$$\mathbf{F}'(\mathbf{h}') = \begin{bmatrix} \lambda(1+\boldsymbol{\kappa}\times\mathbf{h}'\cdot\mathbf{t}) & & \\ \lambda\boldsymbol{\kappa}\times\mathbf{h}'\cdot\mathbf{n} & \frac{1}{\sqrt{\lambda}}\left(1-\frac{1}{2}\boldsymbol{\kappa}\times\mathbf{h}'\cdot\mathbf{t}\right) & \\ \lambda\boldsymbol{\kappa}\times\mathbf{h}'\cdot\mathbf{b} & & \frac{1}{\sqrt{\lambda}}\left(1-\frac{1}{2}\boldsymbol{\kappa}\times\mathbf{h}'\cdot\mathbf{t}\right) \end{bmatrix} + o(h). \quad \text{(S2.4)}$$

This is identical to (3.5). Consequently, the choice of the centerline is unimportant for the first order theory. To ensure the difference between (S2.4) and (3.5) is indeed small, we look at the difference at $O(h^2)$ order, which gives

$$O(h^2) = O(|\boldsymbol{\kappa}\times\mathbf{h}|^2) - \frac{\partial\lambda}{\partial s}\begin{bmatrix} \frac{1}{\lambda^{3/2}}\boldsymbol{\kappa}\times\mathbf{d}\cdot\mathbf{h} & & \\ & -\frac{1}{2}\frac{1}{\lambda^3}\boldsymbol{\kappa}\times\mathbf{d}\cdot\mathbf{h} & \\ & & -\frac{1}{2}\frac{1}{\lambda^3}\boldsymbol{\kappa}\times\mathbf{d}\cdot\mathbf{h} \end{bmatrix}. \quad \text{(S2.5)}$$

To make sure (S2.5) is negligible comparing to (S2.4) we need:

1. $|\boldsymbol{\kappa}\times\mathbf{h}| \ll 1$; and
2. $\partial\lambda/\partial s\,|\mathbf{h}| \ll 1$.

These are our criteria for a jet to be considered thin. Note that the second criterion is only necessary if the deformation of the jet is dominated by twisting, since otherwise $\boldsymbol{\kappa}\times\mathbf{d}\cdot\mathbf{h} \ll \boldsymbol{\kappa}\times\mathbf{d}\cdot\mathbf{t}$ and the second term in (S2.5) is negligible.

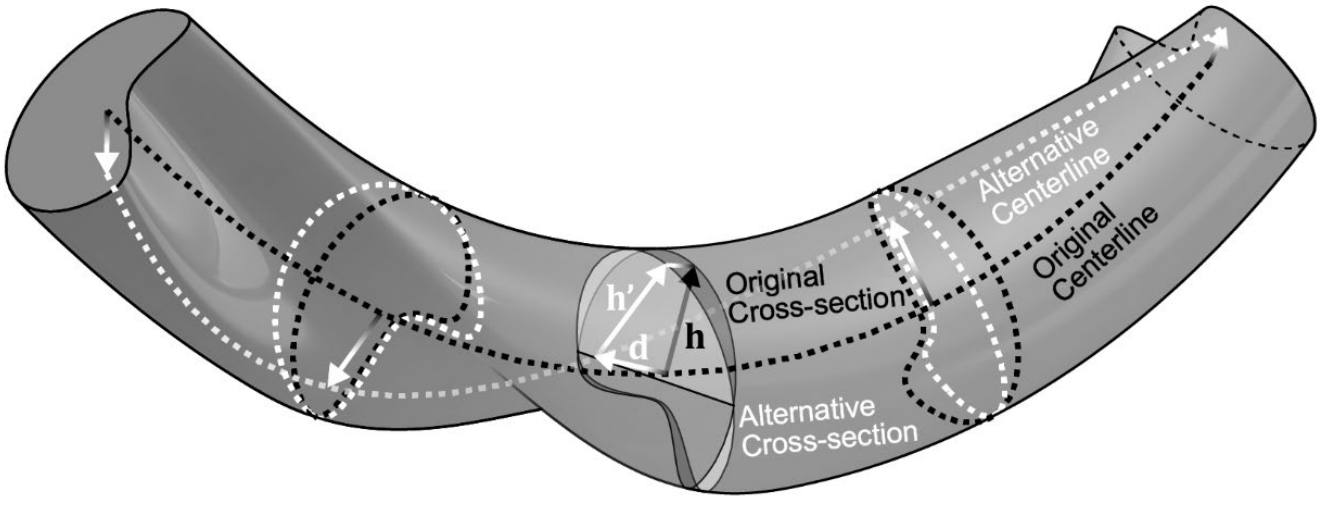

Figure S1. Consider a new centerline that is offset by $\mathbf{d}$ from the original centerline, the cross-section normal to the new centerline may be tilted from the cross-section normal to the original centerline. An offset $\mathbf{h}'$ in the new cross-section then can be decomposed into an offset in the original cross-section $\mathbf{h}$, and a shift along the original centerline.

3. Derivation of the velocity gradient

We obtain the velocity gradient in the local frame by substituting (3.1) into (3.6), which gives

$$\mathbf{L} = \mathbf{W} + \mathbf{R}\mathbf{L}^*\mathbf{R}^{-1}. \tag{S3.1}$$

Here $\mathbf{W} = \dot{\mathbf{R}}\mathbf{R}^{-1}$ is the rotation rate of the local frame and $\mathbf{L}^* = \dot{\mathbf{F}}^*\mathbf{F}^{*-1}$ is the velocity gradient in the local frame. The rotation rate of the local frame $\mathbf{W}$ is characterized by the angular velocity vector $\boldsymbol{\omega}$, which in the matrix form is

$$\mathbf{W} = \begin{bmatrix} & -\omega_b & \omega_n \\ \omega_b & & -\omega_t \\ -\omega_n & \omega_t & \end{bmatrix}. \tag{S3.2}$$

To get the velocity gradient in the local frame, we substitute (3.2) into $\mathbf{L}^* = \dot{\mathbf{F}}^*\mathbf{F}^{*-1}$ and get

$$\mathbf{L}^*(\mathbf{h}) = \mathbf{H}\mathbf{L}^*(\mathbf{0})\mathbf{H}^{-1} + \dot{\mathbf{H}}\mathbf{H}^{-1}. \tag{S3.3}$$

For the first term on the right-hand-side, we can easily write out $\mathbf{L}^*(\mathbf{0}) = \dot{\mathbf{F}}^*(\mathbf{0})\mathbf{F}^{*-1}(\mathbf{0})$ using (3.3). Since $\partial u/\partial s = \dot{\lambda}/\lambda$, we have

$$\mathbf{L}^*(\mathbf{0}) = \begin{bmatrix} \dfrac{\partial u}{\partial s} & & \\ & -\dfrac{1}{2}\dfrac{\partial u}{\partial s} & \\ & & -\dfrac{1}{2}\dfrac{\partial u}{\partial s} \end{bmatrix}. \tag{S3.4}$$

Here $\partial u/\partial s$ is the stretching rate on the centerline, and $-\frac{1}{2}\frac{\partial u}{\partial s}$ represents the decreasing in the cross-section area perpendicular to the centerline as required by material incompressibility.

We need an expression for $\dot{\mathbf{H}}$ to write out the second term on the right-hand-side of (S3.3). We first decompose $\dot{\mathbf{H}}$ into the change in the local frame, $D^*\mathbf{H}/Dt$, and the change due to the rotation of the local frame. Here $D^*\mathbf{H}/Dt$ is known as corotation derivative in continuum mechanics and has the expression [1]

$$\dot{\mathbf{H}} = \frac{D^*\mathbf{H}}{Dt} + \mathbf{W}\mathbf{H} + \mathbf{H}\mathbf{W}^T. \tag{S3.5}$$

Since the basis vectors $\mathbf{t}, \mathbf{n}, \mathbf{b}$ remain constant under D^*/Dt. From (3.4) we have

$$\frac{D^*\mathbf{H}}{Dt} = \begin{bmatrix} \frac{D^*}{Dt}(\boldsymbol{\kappa}\times\mathbf{h})\cdot\mathbf{t} & & \\ \frac{D^*}{Dt}(\boldsymbol{\kappa}\times\mathbf{h})\cdot\mathbf{n} & -\frac{1}{2}\frac{D^*}{Dt}(\boldsymbol{\kappa}\times\mathbf{h})\cdot\mathbf{t} & \\ \frac{D^*}{Dt}(\boldsymbol{\kappa}\times\mathbf{h})\cdot\mathbf{b} & & -\frac{1}{2}\frac{D^*}{Dt}(\boldsymbol{\kappa}\times\mathbf{h})\cdot\mathbf{t} \end{bmatrix} + o(h), \tag{S3.6}$$

with

$$\frac{D^*\boldsymbol{\kappa}}{Dt} = \frac{D\boldsymbol{\kappa}}{Dt} - \boldsymbol{\omega}\times\boldsymbol{\kappa}, \tag{S3.7}$$

$$\frac{D^*\mathbf{h}}{Dt} = \mathbf{v}(\mathbf{h}) - \mathbf{v} - \boldsymbol{\omega}\times\mathbf{h}. \tag{S3.8}$$

Equations (S3.7-S3.8) simply take the rotation of the $\mathbf{t}, \mathbf{n}, \mathbf{b}$ frame out from the material derivative of $\boldsymbol{\kappa}$ and $\mathbf{h}$. Here $\mathbf{v}(\mathbf{h})$ is the velocity of the material point at $\mathbf{h}$, and $\mathbf{v}$ is the velocity on the centerline. By definition $\mathbf{v}(\mathbf{h})$ can be integrated from the velocity gradient, which gives

$$\mathbf{v}(\mathbf{h}) = \mathbf{v} + \int_{\mathbf{0}}^{\mathbf{h}} \mathbf{L}d\mathbf{h}. \tag{S3.9}$$

Since $\mathbf{L}$ also depends on $\mathbf{v}(\mathbf{h})$ through equation (S3.8), equation (S3.9) is an integral equation of $\mathbf{v}(\mathbf{h})$. It is easy to verify that

	$$\mathbf{v}(\mathbf{h}) = \mathbf{v} + \boldsymbol{\omega} \times \mathbf{h} - \frac{1}{2}\frac{\partial u}{\partial s}\mathbf{h} + o(h).$$	(S3.10)

Now we can cancel out $\mathbf{v}(\mathbf{h})$ from (S3.8) using (S3.10), which gives

	$$\frac{D^*\mathbf{h}}{Dt} = -\frac{1}{2}\frac{\partial u}{\partial s}\mathbf{h} + o(h).$$	(S3.11)

Substituting (S3.7) and (S3.11) into equation (S3.6) yields the full expression of $\dot{\mathbf{H}}$, which allows us to write out $\mathbf{L}^*$ by (S3.3).

4. Common form of the Oldroyd-B model

Introduce the short notation for upper-convected derivative

	$$\mathbf{B}_e^{*\nabla} = \frac{D^*\mathbf{B}_e^*}{Dt} - \mathbf{L}^*\mathbf{B}_e^* - \mathbf{B}_e^*\mathbf{L}^{*T}.$$	(S4.1)

Define the deformation rate by

	$$\mathbf{D}^* = \frac{1}{2}(\mathbf{L}^* + \mathbf{L}^{*T}).$$	(S4.2)

Define the deviatoric stress by

	$$\boldsymbol{\tau}^* = \boldsymbol{\sigma}^* - p\mathbf{I}.$$	(S4.3)

We can then rewrite (4.7-4.8) as:

	$$\mu(\mathbf{B}_e^* - \mathbf{I}) = -\zeta\mathbf{B}_e^{*\nabla},$$	(S4.4)
	$$\boldsymbol{\tau}^* = \mu(\mathbf{B}_e^* - \mathbf{I}) + 2\eta\mathbf{D}^*.$$	(S4.5)

Cancel out $\mathbf{B}_e^*$ from the above two equations, we get

	$$\boldsymbol{\tau}^* + \frac{\zeta}{\mu}\boldsymbol{\tau}^{*\nabla} = 2\eta\mathbf{D}^* + 2\frac{\eta\zeta}{\mu}\mathbf{D}^{*\nabla} - \zeta\mathbf{I}^{\nabla}.$$	(S4.6)

Note that by definition (S4.1) and (S4.2), we have

	$$\mathbf{I}^{\nabla} = -\mathbf{L}^* - \mathbf{L}^{*T} = -2\mathbf{D}.$$	(S4.7)

Plug (S4.7) into (S4.6) we get

	$$\boldsymbol{\tau}^* + \frac{\zeta}{\mu}\boldsymbol{\tau}^{*\nabla} = 2(\eta+\zeta)\left(\mathbf{D}^* + \frac{\eta\zeta}{\mu(\eta+\zeta)}\mathbf{D}^{*\nabla}\right).$$	(S4.6)

Define relaxation times $\lambda_1 = \zeta/u$ and $\lambda_2 = \lambda_1\eta/(\eta+\zeta)$, (S4.6) assumes the common form appeared in rheology textbooks [2]:

	$$\boldsymbol{\tau}^* + \lambda_1\boldsymbol{\tau}^{*\nabla} = 2(\eta+\zeta)\left(\mathbf{D}^* + \lambda_2\mathbf{D}^{*\nabla}\right).$$	(S4.7)

We have avoided this common form of the Oldroyd-B model since the upper-convected derivative of stress would cause unnecessary complexity when integrating for the total force and the total torque in the jet.

5. Modeling the rotary jet spinning

For simplicity, we only model the steady state of a jet in rotary jet spinning. Gravity, air-drag, solvent evaporation, and solidification of the jet are neglected. Under these assumption, the mass conservation (5.2) simplifies to

	$$\frac{\partial}{\partial s}(\rho A u) = 0.$$	(S5.1)

Assume the volume flow rate through the orifice to be Q. Equation (S5.1) can be trivially integrated to obtain

	$$Au = Q.$$	(S5.2)

Note that the local frame is rotating with the reservoir, the momentum balance (5.4) in the local frame becomes

	$$\frac{\partial}{\partial s}(u\rho A\mathbf{v}) = \frac{\partial \mathbf{f}}{\partial s} + \rho A\boldsymbol{\Omega} \times (\boldsymbol{\Omega} \times \mathbf{r}) - 2\rho A\boldsymbol{\Omega} \times \mathbf{v}.$$	(S5.3)

Here we locate the origin of the lab frame at the center of the reservoir so that $\mathbf{r}$ as defined in section 1 is the distance from the center of the reservoir. $\boldsymbol{\Omega}$ is the rotation rate of the reservoir. $\rho A\boldsymbol{\Omega} \times (\boldsymbol{\Omega} \times \mathbf{r})$ is the centrifugal force. $2\rho A\boldsymbol{\Omega} \times \mathbf{v}$ is the Coriolis force. At steady state the angular momentum balance (5.7) simplifies to

	$$u\frac{\partial}{\partial s}(\rho \mathbf{J}\boldsymbol{\omega}) + \frac{\partial}{\partial s}\big(2u\rho \mathbf{J}(\boldsymbol{\Omega} + \boldsymbol{\omega})\big) = \mathbf{t} \times \mathbf{f} + \frac{\partial \mathbf{M}}{\partial s}.$$	(S5.4)

In practice the jet exits the orifice perpendicular to the rotation axis [3]. With gravity neglected, the jet stays in a 2D plane perpendicular to the rotation axis. If we choose the local bases such that $\mathbf{b}$ is in the direction of $\boldsymbol{\Omega}$, $\mathbf{t}$ is tangent to the jet, $\mathbf{n} = \mathbf{b} \times \mathbf{t}$ is normal to the jet, then the jet only moves in the $\mathbf{t}, \mathbf{n}$ plane, Fig.3A, and (S5.3-S5.4) consist of three equations:

	$$\rho Q\frac{\partial u}{\partial s} = \frac{\partial f_t}{\partial s} - f_n\kappa + \rho A\Omega^2 r\cos\theta,$$	(S5.5)
	$$\rho Qu\kappa = \frac{\partial f_n}{\partial s} + f_t\kappa + \rho A\Omega^2 r\sin\theta - 2\rho A\Omega u, \text{and}$$	(S5.6)
	$$\frac{\partial}{\partial s}\big(2u\rho J_{bb}(\Omega + \omega)\big) = f_n + \frac{\partial M}{\partial s}.$$	(S5.7)

Here $\Omega, \omega, \kappa, M$ are all in the $\mathbf{b}$ direction. θ is the angle between $\mathbf{t}$ and $\mathbf{R}$.

For the stretch of the polymer chains, the evolution equation (4.10) becomes

	$2u\frac{\partial \lambda_{e\parallel}}{\partial s} - 2\lambda_{e\parallel}\frac{\partial u}{\partial s} = -\frac{\mu}{\zeta}\left(\lambda_{e\parallel} - \frac{1}{\lambda_{e\parallel}}\right)$, and	(S5.8)
	$2u\frac{\partial \lambda_{e\perp}}{\partial s} + \lambda_{e\perp}\frac{\partial u}{\partial s} = -\frac{\mu}{\zeta}\left(\lambda_{e\perp} - \frac{1}{\lambda_{e\perp}}\right)$.	(S5.9)

For the gradient of the stretch of the polymer chains across the cross-section, since the jet only moves in the $\mathbf{t}, \mathbf{n}$ plane, in (4.13) $\boldsymbol{\beta} = \beta_b \mathbf{b}$. Then (4.11) becomes

	$u\frac{\partial \beta_b}{\partial s} - \frac{5}{2}\beta_b\frac{\partial u}{\partial s} = -\frac{\mu}{\zeta}\beta_b + \left(2u\frac{\partial \kappa_b}{\partial s} - \kappa\frac{\partial u}{\partial s}\right)\lambda_{\parallel}^2$, and	(S5.10)
	$u\frac{\partial \chi}{\partial s}\beta_b + u\chi\frac{\partial \delta_b}{\partial s} + \frac{1}{2}\chi\beta_b\frac{\partial u}{\partial s} = -\frac{\mu}{\zeta}\chi\beta_b - \left(u\frac{\partial \kappa}{\partial s} - \frac{\kappa}{2}\frac{\partial u}{\partial s}\right)\lambda_{\perp}^2$.	(S5.11)

The total force in the jet, according to (4.16), is

	$f_t = \mu A\left(\lambda_{e\parallel}^2 - \lambda_{e\perp}^2\right) + 3\eta A\frac{\partial u}{\partial s}$.	(S5.12)

As mentioned earlier, f_n is of higher order and is not predicted by the constitutive relation. The torque in the jet, according to (4.17), is

	$M = J_{bb}\mu(1-\chi)\beta_b + 3J_{bb}\eta\left(u\frac{\partial \kappa}{\partial s} - \frac{\kappa}{2}\frac{\partial u}{\partial s}\right)$.	(S5.13)

The governing equations are closed by the steady state kinematic condition (S1.5): $\omega = u\kappa$, which says that the rotation of the material (ω) is solely caused by traveling (u) along a curve (κ), and the assumption of circular cross-section: $A = \pi a^2$ and $J_{bb} = \pi a^4/4$, where a is the radius of the jet.

As the boundary conditions, we specify the initial velocity of the jet v_0 at the orifice and the volumetric flow rate Q. The velocity is assumed to be normal to the orifice. The initial radius of the jet is then determined by $a_0 = \sqrt{Q/\pi v_0}$. The distance from the orifice to the center of the reservoir is the radius of the reservoir r_0. We assume that the jet has no bending at the orifice: δ_b, χ, κ vanish. We assume

that the jet is at steady state stretching at the orifice: $\partial\lambda_{\parallel}/\partial s$ and $\partial\lambda_{\perp}/\partial s$ vanish. We assume that the jet is stress-free at the downstream end: f_t, f_n, M_b vanish. Since we simulate for a fixed arc-length of the jet, the stress-free boundary condition downstream does not correspond to the free-moving end of the jet. Instead, it approximates the point where the stress has been fully relaxed. Since our material only has finite memory of the loading history, this approximation has negligible effect on the trajectory far away from the downstream end. To exclude the effect of jet length on our study, we simulate for a very long jet (arc length range $s \in [0,100r_0]$) but only plot the solution for a relatively short range $s \in [0,10r_0]$.

The problem is governed by five dimensionless groups: the Reynolds number $Re = \rho v_0 r_0/\zeta$ characterizing the competition between inertia and the viscoelasticity in the jet, the Rossby number $Ro = v_0/\Omega r_0$ characterizing the effect of centrifugal force and Coriolis force, the Weissenberg number for the polymer part and the solvent part $Wi_p = \zeta v_0/\mu r_0$ and $Wi_s = \eta v_0/\mu r_0$, characterizing the viscoelastic relaxation in the jet, and the slenderness ratio $Sl = a_0/r_0$, comparing the resistance to the bending of the jet versus the resistant to the stretching of the jet.

We solve the system of ordinary differential equations in Matlab using the function bvp4c. We choose our simulation condition to represent common spinning condition by fixing $Re = 1$, $Ro = 0.1$, $Wi_s = 10^{-2}$, $Sl = 10^{-2}$ [4]. We study the effect of the viscoelasticity of the polymer jet by varying $Wi_p = 0.01, 0.1, 1$ in Fig.4.

6. Steady state of an eventually elastic jet

Consider an eventually elastic jet at its steady state. Here by "eventually elastic" we mean that although the jet may show short time viscoelastic behavior, given long enough relaxation time, the jet will eventually relax to an elastic deformation. Since elasticity propagates tension all the way through the jet, the only way that an elastic jet can be at steady state is that when certain amount of material comes out

from the orifice, the same amount of materials becomes stress-free at the free-moving end of the jet, and the part of the jet with tension remains constant. Over time, there will be an infinite amount of stress-free jet accumulated. In this section we focus on the study of this stress-free region of the jet.

Put stress-free condition into the momentum balance equations (S5.5-S5.6), we get

	$$\rho Q \frac{\partial u}{\partial s} = \rho A \Omega^2 r \cos\theta,$$	(S6.1)
	$$\rho Q u \kappa = \rho A \Omega^2 r \sin\theta - 2\rho A \Omega u.$$	(S6.2)

Note that a perfect elastic jet implies $u = v_0$ and $\partial u/\partial s = 0$ at stress-free state. Then (S6.1) gives $\cos\theta = 0$, which means that the stress-free jet forms a circular ring. We can visualize the trajectory of an elastic jet in Fig.S2. The circular shape implies $\kappa = 1/r$. Consequently, (S6.2) becomes

	$$\frac{v_0^2}{r} = \Omega^2 r - 2\Omega v_0.$$	(S6.3)

This equation has a unique solution $r_{end} = v_0/\Omega$. This solution means that the ring is motionless if viewed in the lab frame not rotating with the reservoir. Recall the definition of the Rossby number $Ro = v_0/\Omega r_0$. When $Ro < 1$, we have $r_{end} < r_0$, which means that the jet would fall onto the reservoir. In fact, falling of jet onto fast rotating reservoir has previously been observed in experiment [5].

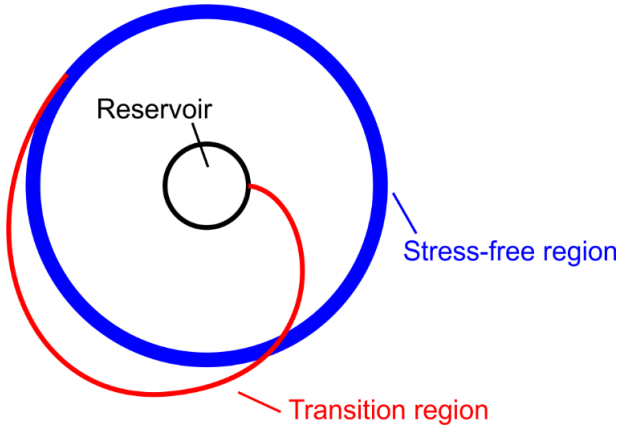

Figure S2. The trajectory of an eventually elastic jet at the steady state consists of two parts: a transitional region with varying tension along the jet, and a stress-free region that collapses onto a thick ring. The transition region may have a complex trajectory depending on the possible viscoelastic property of the jet.

7. List of symbols

Notation list

$O(h)$	Any term that is first order in $\mathbf{h}$ in an asymptotic expansion
$o(h)$	Any term that is higher than first order in $\mathbf{h}$ in an asymptotic expansion
$\delta(\ \ )$	The $O(h)$ order terms of a variable in an asymptotic expansion
$(\ \ )^*$	Variable in the local frame
$\frac{D^*}{Dt}$	Material derivative in the local frame

Variable list (in alphabetic order, Latin followed by Greek)

a	The radius of the jet
a_0	The radius of the orifice
A	Cross-section area of the jet
$\mathbf{b}$	One of the basis vectors of the local frame, with the definition $\mathbf{b} = \mathbf{t} \times \mathbf{n}$.
$\mathbf{B}_e$	Left Cauchy-Green tensor of the elastic deformation, with the definition $\mathbf{B}_e = \mathbf{F}_e\mathbf{F}_e^T$
$\mathbf{f}$	Traction force on a cross-section of the jet, where $f_t = \mathbf{f} \cdot \mathbf{t}$, $f_n = \mathbf{f} \cdot \mathbf{n}$ in section S4
$\mathbf{F}$	Deformation gradient
$\mathbf{F}_e$	Elastic part of the deformation gradient
$\mathbf{F}_v$	Viscous part of the deformation gradient
$\mathbf{H}$	Deformation gradient relative to the center line
$\mathbf{h}$	An offset vector in the cross-section from the centerline, with $h = \lvert\mathbf{h}\rvert$
$\mathbf{I}$	Identity matrix
$\mathbf{J}$	Matrix of the second moment of area of the jet cross-section, with components

	J_{tt},J_{nn},J_{nb},J_{bb}
$\mathbf{L}$	Velocity gradient $\mathbf{L} = \dot{\mathbf{F}}\mathbf{F}^{-1}$
$\dot{m}$	Mass exchange per unit length of the jet
$\mathbf{m}_{bend}$	Shorthand for $\mathbf{m}_{bend} = \mu(1-\chi)\boldsymbol{\delta} + 3\eta\left(\frac{D^*\boldsymbol{\kappa}}{Dt} - \frac{1}{2}\frac{\partial u}{\partial s}\boldsymbol{\kappa}\right)$
$\mathbf{m}_{twist}$	Shorthand for $\mathbf{m}_{twist} = \mu\boldsymbol{\delta} + \eta\frac{\partial \boldsymbol{\omega}}{\partial s}$
$\mathbf{M}$	Torque on a cross-section of the jet, where $\mathbf{M} = M\mathbf{b}$ in section S4
$\mathbf{n}$	A normal vector of the centerline
p	Hydrostatic pressure experienced by the viscoelastic material
$\mathbf{q}$	Body force experienced by the jet
Q	Volumetric flow rate through the orifice
$\mathbf{r}$	Location of the jet as defined by material points on the centerline
r_0	The radius of the reservoir
$\mathbf{R}$	Rotation matrix that transforms between the lab frame and the local frame
s	Arc length along the centerline from the orifice
t	Time
$\mathbf{t}$	Tangent vector of the centerline
u	Velocity of the jet along the centerline, $u = \mathbf{v}\cdot\mathbf{t}$
$\mathbf{v}$	Velocity of the jet
$\mathbf{W}$	Rotation rate of the local frame relative to the lab frame, $\mathbf{W} = \dot{\mathbf{R}}\mathbf{R}^{-1}$
$\boldsymbol{\beta}$	A vector introduced to define the first order asymptotic terms of $\mathbf{B}_e$
ζ	Viscosity due to polymer chains sliding apart
η	Viscosity due to solvent molecules sliding apart
θ	Angel between the centrifugal force and the tangent vector $\mathbf{t}$
$\boldsymbol{\kappa}$	Curvature vector of the centerline of the jet, where $\boldsymbol{\kappa} = \kappa\mathbf{b}$ in section S4

λ	Stretch of the material on the centerline relative to the reference state
$\lambda_{e\parallel}, \lambda_{e\perp}$	Components of the zeroth order asymptotic terms of $\mathbf{B}_e$
μ	Elastic modulus of the stretching of polymer chains
ρ	Density of the polymer solution
$\boldsymbol{\sigma}$	Stress tensor
$\boldsymbol{\sigma}_e$	Stress due to the elastic deformation of the polymer chains
$\boldsymbol{\sigma}_s$	Stress due to the deformation of solvent
$\boldsymbol{\sigma}_v$	Stress due to the viscous deformation of the polymer chains
χ	A variable introduced to define the first order asymptotic terms of $\mathbf{B}_e$
$\boldsymbol{\omega}$	Angular velocity on the centerline of the jet, where $\boldsymbol{\omega} = \omega\mathbf{b}$ in section S4
$\boldsymbol{\Omega}$	The rotation vector of the reservoir, with the assumption $\boldsymbol{\Omega} = \Omega\mathbf{b}$

Reference

1. Irgens, F., *Continuum mechanics*. 2008: Springer Science & Business Media.
2. Owens, R.G. and T.N. Phillips, *Computational rheology*. Vol. 14. 2002: World Scientific.
3. Badrossamay, M.R., et al., *Nanofiber assembly by rotary jet-spinning.* Nano letters, 2010. **10**(6): p. 2257-2261.
4. Mueller, B., *Additive manufacturing technologies–Rapid prototyping to direct digital manufacturing.* Assembly Automation, 2012. **32**(2).
5. Badrossamay, M.R., et al., *Engineering hybrid polymer-protein super-aligned nanofibers via rotary jet spinning.* Biomaterials, 2014. **35**(10): p. 3188-3197.